Powder Technology 188 (2008) 110–118

Contents lists available at ScienceDirect

Powder Technology

journal homepage: www.elsevier.com/locate/powtec

Behaviour of a curtain of particles falling through a horizontally-flowing gas stream

Chrestella Wardjiman [a], Andrew Lee [b], Madoc Sheehan [b], Martin Rhodes [a,*]

[a] Department of Chemical Engineering, Monash University, Victoria 3800, Australia
[b] James Cook University, School of Engineering, Townsville, Queensland 4811, Australia

ARTICLE INFO

Article history:
Received 13 September 2007
Received in revised form 4 March 2008
Accepted 9 April 2008
Available online 16 April 2008

Keywords:
Particle curtain
Trajectory
Solid particles
Cross-flow

ABSTRACT

With a view to an application in heat recovery from hot gases, the fluid dynamics of a curtain of particles falling in a horizontal gas stream was studied. Air with a uniform velocity profile flowed through a duct with cross-section of 0.15×0.60 m. A stream of sand particles, with a mean diameter of 204 μm and density of 2640 kg/m^3, was fed into the duct from above to form a curtain across the entire width of the duct. The particle flowrates ranged from 0.031 to 0.047 kg/s. The inlet particle curtain thickness in the direction of the gas flow ranged from 0.02 to 0.10 m, and the horizontal air velocity was varied from zero to 1.2 m/s. In an experimental study, the trajectory of the particle curtain was tracked using high-speed video camera and the velocity profile of the air downstream of the curtain was measured using a pitot tube. The fluid dynamic behaviour of the particle curtain was analysed using a Eulerian–Eulerian computational fluid dynamics (CFD) model that is capable of predicting the complete flow fields of the gas and particles. Also, a simple single particle model was used to predict the particle velocity at the centerline and trajectories of the leading and trailing edges of the particle curtains falling in a horizontal air flow. Good agreement was found between the experiments and the CFD model predictions. However, predictions from the simple single particle model were less satisfactory due primarily to the non-uniform gas flow found in practice, compared to the assumed uniform flow.

1. Introduction

There is an increasing industrial interest in gas-solid contacting techniques, which reduce reaction time, improve product quality, reduce waste, and environmental impact [1]. One interesting technique that has received attention is a system with a falling curtain of particles in a gas stream. This technique has been used in many areas such as granulation, drying, heat transfer and chemical reaction.

For example in the granulation of urea, the molten urea is sprayed onto cascading granules in a rotary drum to build seed granules to product size [2]. As the melt strikes the surface of the granules, it quickly solidifies forming a coating. Wegerer [21] patented a short contact time process that involves a falling curtain of catalyst. In the reactor, the feed is sprayed horizontally onto the falling curtain of catalyst. The feed transversely contacts the curtain of falling catalyst particles. Hruby et al. [3] used free-fall particles as direct absorbers of the solar energy. In all of the above examples, a good contact between gas and particle is essential.

Numerous investigations have been conducted to understand the flow characteristic of free-falling particle curtain in quiescent air and cross-flow gas. For example, Hruby et al. [3] investigated the flow characteristics of a free-falling spherical particle curtain in quiescent air. The particle curtain was generated by causing particles to fall through a rectangular slit in the base of a hopper. Experimental results showed that the particles in the curtain fall faster than a single isolated spherical particle falling in quiescent surroundings. Hruby et al. postulated that when a curtain of spherical particles falls freely under gravity through the quiescent air, the surrounding air is entrained into the particle curtain and that this results in a vertically downward air velocity. Hruby et al. suggested that this caused the falling particle velocities in the curtain to be higher than the free-falling velocity of an isolated sphere in quiescent air. Hruby et al. also observed that an increase in solid mass flowrate leads to a higher particle velocity. The authors suggested that the higher solid mass flowrate results in more air entrainment (i.e. increased downward air velocity in the curtain) that subsequently augmented the particle velocities. These trends were also observed by Uchiyama [4] and Ogata et al. [5] in their study of a free-falling particle jet in unbounded air. The particle jet was generated by an orifice outlet located at the bottom of a hopper.

Ogata et al. [5] compared the measured centerline velocity of the particle jet in quiescent air with the velocity of a single particle falling without drag. The results showed that the measured velocity near to the orifice follows closely that for a single particle without drag. As the particles fall further, the model underpredicts the measured velocity. Ogata et al. suggested that this is due to the high particle–particle interaction and small relative velocity between particle and air (i.e. resulting in low fluid drag) near to the orifice. As the particles fall further, the particles accelerate freely under gravity.

* Corresponding author.
E-mail address: rhodes@eng.monash.edu.au (M. Rhodes).

0032-5910/$ – see front matter © 2008 Elsevier B.V. All rights reserved.
doi:10.1016/j.powtec.2008.04.002

The study of a free-falling particle curtain in a horizontal gas flow appears in numerous rotary drum studies. The interior surface of the drum is usually fitted with flights which elevate the particles and allow them to cascade through the gas stream as the drum rotates. The cascading particles form curtains which are parallel to the length of the drum. Free spaces are generated in between the cascading curtains. The gas stream flows parallel to the main plane of the particle curtains.

Kelly and O'Donnell [6] and Kamke and Wilson [7] investigated the flow characteristic of particle curtains in the rotary drum. The authors suggested that when a particle curtain falls in a horizontal gas flow, particles fall as sheets where the falling particles within the curtain are shielded from the horizontal gas flow. The experimental results were compared with the predictions of a model which assumed that the particles fall independently of one another (i.e. with no particle–particle interaction). However, Kelly and O'Donnell's model over-estimated the displacement of the falling particles. The authors suggested it was due to the particles being partially shielded from the main gas stream. Later, Kelly and O'Donnell [8] were able to take into account the shielding effect in the rotary drum by assuming an above-average gas velocity in the free space between the particle curtains. This meant the gas velocity within the falling curtain of particles was below the average value. Having a lower gas velocity within a falling particle curtain enabled Kelly and O'Donnell to correctly predict the displacement of the falling particles.

In another study, Sherritt et al. [9] investigated the mean horizontal displacement of a particle curtain falling through a horizontal flowing gas stream produced in a wind tunnel. The falling particle curtain occupied only a portion of the width of the gas stream in the wind tunnel. The direction of the gas flow was parallel to the plane of the curtain. Some of the gas flow through the particle curtain while most of the gas would flow on either side of the curtain. Their observations support the work of Kelly and O'Donnell [8] where the gas velocity within the particle curtain is reported to be lower than the average velocity.

As the above studies showed, most of the gas flows in the free space between the particle curtains instead of flows through the curtain, therefore reducing the contact efficiency between gas and solid. In the present study, a particle curtain is generated to span across the *entire* width of the vessel and the gas flow is horizontal and perpendicular to the main plane of the curtain. Since there is no free space between the wall and the particle curtain, gas is forced to flow through the curtain. The aim of this study was to investigate the fluid dynamic behaviour of the particle curtain under these conditions. This investigation is part of a larger study to determine the feasibility of using the particle curtain as a heat exchanger. In modelling the fluid dynamic behaviour of the particle curtain computational fluid dynamics (CFD) has been used.

CFD has successfully been used to model a wide range of gas–solids systems, such as fluidized beds (for example Du et al. [10] and Nakamura and Watano [11]) and pneumatic conveying (for example Hidayat and Rasmuson [12]). A number of different approaches have been developed for simulating two-phase gas–solids systems, for example Eulerian–Eulerian and Eulerian–Lagrangian approaches, each appropriate for a specific set of circumstances. In situations involving large numbers of particles, the Lagrangian methods of tracking individual particles are often prohibitive, thus the Eulerian–Eulerian approach is generally used for large systems [13].

2. Experimental

2.1. Particle curtain apparatus

A schematic diagram of the experimental setup is shown in Fig. 1. The apparatus consisted of the following parts: a duct, air supply system, solid feeder, solid transport system, collection drum, and measurement system. The duct had cross-sectional dimensions of 0.15 m width, 0.60 m height and a length of 2.40 m in the direction of air flow. The side walls of the duct were made of transparent Perspex. At the base of the duct, slots which could be opened or closed were installed to create a smooth wall at the bottom of the duct. During each experiment, most of the slots were closed, except those at the specific location where the particle curtain lands.

The airflow to the vessel was provided by a Rootes-type positive displacement blower. In order to minimise the gas swirl before entering

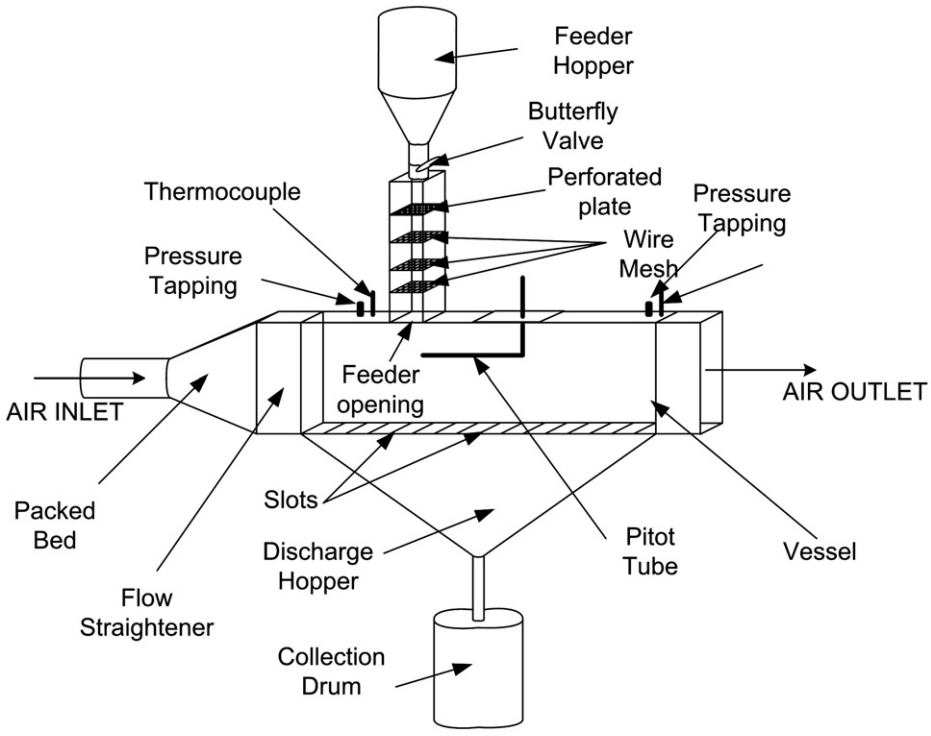

Fig. 1. A schematic diagram of the experimental setup.

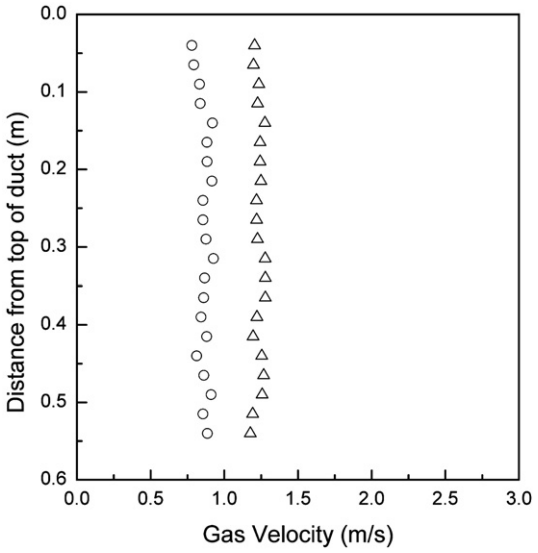

Fig. 2. Air velocity profile measured 30 cm from the inlet of duct (○ — mean air velocity of 0.9 m/s and Δ — mean air velocity of 1.2 m/s).

the vessel, a packed bed was installed in the transformation section connecting the 150 mm diameter pipe to the rectangular entrance to the vessel. The packed bed was made from randomly-packed, 25 mm lengths of 25 mm i.d PVC tube with 2 mm wall thickness. A flow straightener was installed immediately downstream of the packed bed to produce an even gas velocity distribution across the vessel cross-section. Fig. 2 showed the typical air velocity profile where there was no solids flow inside the duct. The volumetric flowrate of the air was measured with an orifice plate positioned upstream of the apparatus. In the setting for this investigation, the gas velocity in the vessel could be varied from zero to 2.4 m/s.

A curtain of particles with steady mass flow rate and uniform particle distribution was created by steadily feeding solids from a hopper through a rectangular feeder in which a perforated plate and three pieces of wire mesh are secured. Uniform and steady curtains with various curtain thicknesses were created by adjusting the dimensions of feeder. The mass flow rate of the particle curtain was varied by controlling the hole size of the perforated plate. The particles stored in the hopper were discharged from the vessel and collected in a collection drum located underneath the vessel. Solids caught in the collection drum after an experiment were transferred back pneumatically to the hopper before the start of the next experiment. The capacity of the hoppers was approximately 500 kg of solid particles. In the setting for this investigation, the particle mass flowrate could be varied from zero to 0.1 kg/s.

At the start of an experiment the appropriate perforated plate was installed to establish the required mass flowrate. The dimension of the feeder opening was adjusted to the desired size to obtain the initial curtain thickness (in the direction of air flow) at the point where the solids enter the duct [Fig. 3]. The air flowrate was then established by adjusting the opening of the air-purging valve downstream of the blower to allow the correct amount of air passed through the duct. The butterfly valve beneath the solids feed hopper was then opened to allow particles to fall from the hopper. The particles used were silica sand with Sauter mean diameter of 204 μm and a particle density of 2640 kg/m^3.

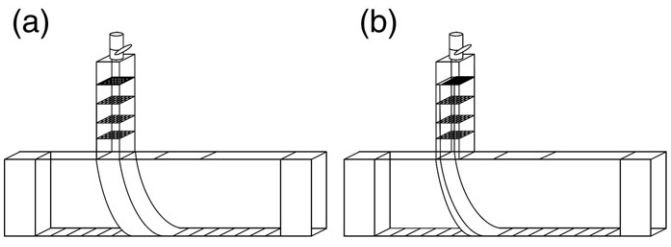

Fig. 3. A schematic diagram of the adjusted inlet curtain thickness (a) 10 cm and (b) 2 cm.

2.2. Measurements

The particle curtain was imaged in an elevation through the Perspex side wall of the duct using a high-speed, digital camera at 1076 fps. The edges of the particle curtain were then tracked frame by frame. Fig. 4 is a typical image of particle curtain showing the tracked leading and trailing edges.

The vertical component of particle velocities at the centerline (judged by eye) of particle curtain were obtained by capturing the individual particle images using a digital high-speed camera at 1930 fps [Fig. 4]. The vertical particle velocities were measured as a function of vertical position in the duct. For each image, the high-speed camera was adjusted to the desired vertical position and the lens's focus is set at the centerline of particle curtain. The position of particles is then tracked frame by frame.

In order to measure the solid flowrate, the collection drum was suspended from a load cell during the experiments. The changes in voltage with time in the load cell were detected and recorded by the data acquisition system for the mass flowrate calculation. The precision of the measurement was ±0.001 kg/s. The gas velocity profile immediately downstream of the particle curtain was measured using a pitot tube connected to a pressure transducer. The tip of the pitot tube could be positioned at the desired location where the gas velocity was to be measured.

3. Modelling

3.1. Simple single particle model

Falling particles inside the vessel form a curtain which spans across the entire width of the vessel and the gas flow are horizontal and perpendicular to the main plane of the curtain. The falling particles are displaced horizontally due to the drag of the gas stream while falling

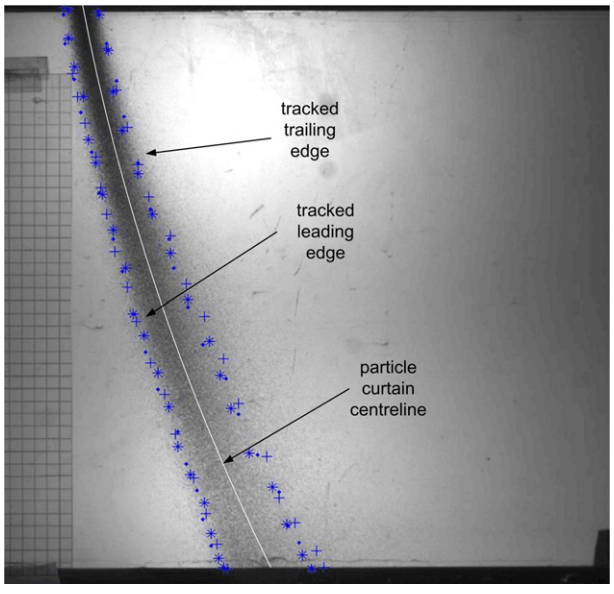

Fig. 4. Image of particle curtain captured at the wall of duct by high-speed camera. Size of the image is 50×50 cm.

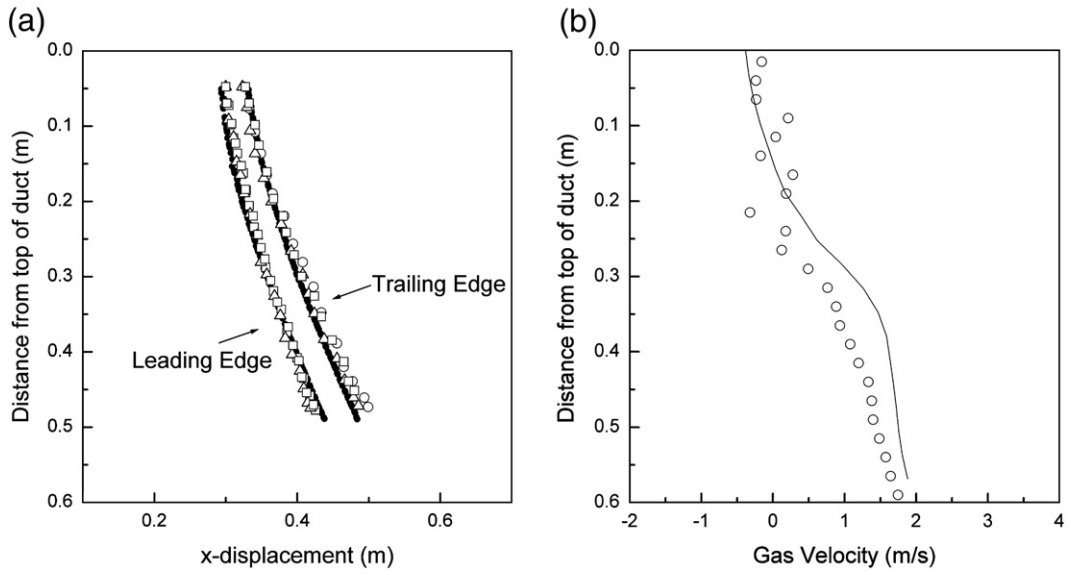

Fig. 5. (a). Particle curtain trajectories for particle curtain with inlet thickness of 2 cm, solid mass flowrate of 0.040 kg/s, and air velocity of 0.9 m/s (○ Run 1, □ Run 2, Δ Run 3, — CFD model). (b). Gas velocity profile at the trailing edge for particle curtain with inlet thickness of 2 cm, solid mass flowrate of 0.040 kg/s, and air velocity of 0.9 m/s (○ measured, — CFD model).

vertically under gravity. In this model, it is assumed that the forces acting on the particle in the horizontal direction are independent of those in the vertical direction. It is also assumed that each particle moves as if in a fluid of infinite extent and that the particle motion is unhindered by the proximity of other particles.

The force balance in horizontal direction for a single particle falling through a horizontally-flowing gas becomes

$$\ddot{x}_p = \frac{3}{4} C_D \frac{\rho_g}{\rho_p d_p} (\dot{x}_p - \dot{x}_g) \left| \dot{x}_p - \dot{x}_g \right| \tag{1}$$

And a force balance in vertical direction for a single particle:

$$\ddot{y}_p = \left(1 - \frac{\rho_g}{\rho_p}\right) g - \frac{3}{4} C_D \frac{\rho_g}{\rho_p d_p} \left(\dot{y}_p - \dot{y}_g\right) \left| \dot{y}_p - \dot{y}_g \right| \tag{2}$$

The drag coefficients for a sphere particle are determined by the following expressions [14].

$$C_D = \frac{24}{\mathrm{Re}}; \mathrm{Re} < 0.2 \tag{3}$$

$$C_D = \frac{24}{\mathrm{Re}} \left(1 + 0.15 \mathrm{Re}^{0.687}\right); 0.2 < \mathrm{Re} < 1000 \tag{4}$$

$$C_D \approx 0.44; 1000 < \mathrm{Re} < 2 \times 10^5 \tag{5}$$

Since it is assumed that the particle motion in the x-direction is independent of that in the y-direction, the drag coefficient in x-direction is also independent of that in the y-direction.

3.2. CFD model

The falling curtain of solids within the moving airstream was simulated using a steady-state solution to the unsteady-state governing equations for a two-phase system using an Eulerian–Eulerian approach. The moving air stream was modelled as a continuous fluid phase and the falling solids as a dispersed phase with interparticle forces. The numerical domain was discretized with a with a 9 mm tetrahedral mesh applied to the region in which the particle curtain existed and extending for a minimum of 50 mm beyond the expected curtain boundaries. The remainder of the vessel was discretized using a maximum mesh size of 35 mm, resulting in a total mesh with of 136,000 nodes. The model was solved using CFX 5.7.1 until all residuals were less than 10^{-4}, or 100 iterations had passed.

The three-dimensional flow behaviour of the gas and solids phases were solved using the Navier–Stokes equations combined with the industry standard $k-\varepsilon$ model [15] for turbulence in the continuous phase and a zero-equation model for the dispersed phase. Different turbulence models were examined and minor differences were observed in the curtain and gas velocity profiles, and thus the $k-\varepsilon$ model was used in the simulations. These equations are given below (the subscript α represents the current phase and β represents the other phase).

Continuity Equation:

$$\frac{\partial}{\partial t}(r_\alpha \rho_\alpha) + \nabla \cdot (r_\alpha \rho_\alpha U_\alpha) = 0 \tag{6}$$

Momentum Equation:

$$\begin{aligned} \frac{\partial (r_\alpha \rho_\alpha U_\alpha)}{\partial t} + \nabla \cdot (r_\alpha (\rho_\alpha U_\alpha \otimes U_\alpha)) = & -r_\alpha \nabla P_\alpha \\ & + \nabla \cdot \left(r_\alpha \mu_\alpha \left(\nabla U_\alpha + (\nabla U_\alpha)^{T_\alpha}\right)\right) \\ & + r_\alpha \rho_\alpha g + g(\rho - \rho_{\mathrm{ref}}) \\ & + \beta (U_\alpha - U_\beta) \end{aligned} \tag{7}$$

where $\beta = \frac{3 \mu_g r_p}{4 d_p^2} \mathrm{Re} \times C_D$ is used to describe the effects of drag forces on the gas.

In addition to the unsteady-state Navier–Stokes equations, the following equations were used to describe the effects of turbulence in the model.

Turbulent Viscosity

$$\mu_{t\alpha} = 0.09 \rho_\alpha \frac{k_\alpha^2}{\varepsilon_\alpha} \tag{8}$$

Continuous Phase Turbulence Model ($k-\varepsilon$ model).

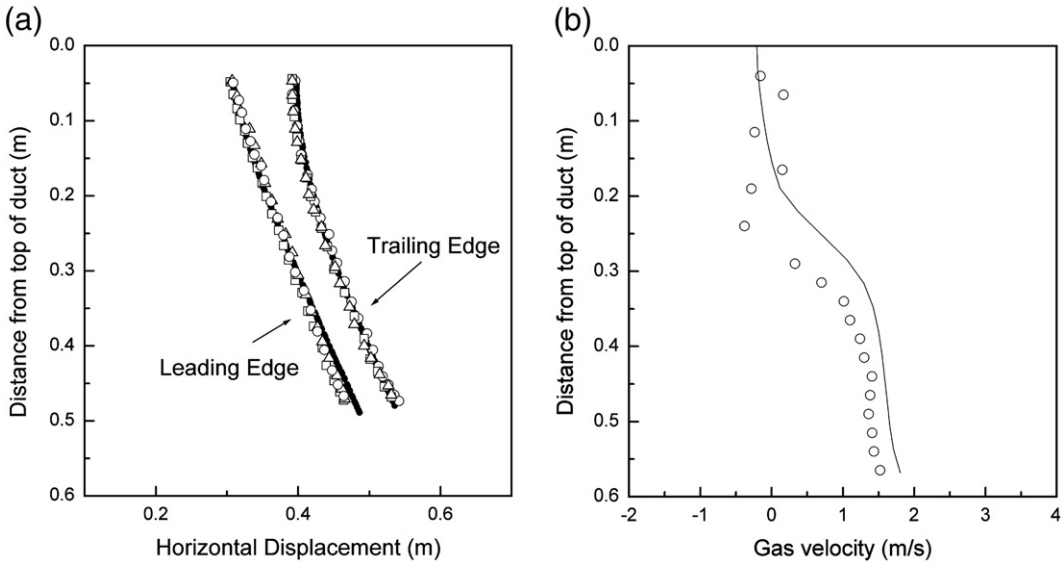

Fig. 6. (a). Particle curtain trajectories for particle curtain with inlet thickness of 10 cm, solid mass flowrate of 0.040 kg/s, and air velocity of 0.9 m/s (○ Run 1, □ Run 2, Δ Run 3, — CFD model). (b). Gas velocity profile at the trailing edge for particle curtain with inlet thickness of 10 cm, solid mass flowrate of 0.040 kg/s, and air velocity of 0.9 m/s (○ measured, — CFD model).

Turbulent Kinetic Energy

$$\frac{\partial}{\partial t}\left(r_g\rho_g k_g\right)+\nabla\cdot\left(r_g\left(\rho_g U_g k_g-\left(\mu+\frac{\mu_{tg}}{\sigma_k}\right)\nabla k_g\right)\right)=r_g\left(P_{kg}-\rho_g\varepsilon_g\right)+T_{gp}^{(k)} \tag{9}$$

Turbulence Dissipation Rate

$$\frac{\partial}{\partial t}\left(r_g\rho_g\varepsilon_g\right)+\nabla\cdot\left(r_g\rho_g U_g\varepsilon_g-\left(\mu+\frac{\mu_{tg}}{\sigma_\varepsilon}\right)\nabla\varepsilon_g\right)=r_g\frac{\varepsilon_g}{k_g}\left(C_{\varepsilon1}P_{kg}-C_{\varepsilon2}\rho_g\varepsilon_g\right)+T_{gp}^{(k)} \tag{10}$$

where $C_{\varepsilon1}=1.44$, $C_{\varepsilon2}=1.92$, $\sigma_k=1.0$ and $\sigma_\varepsilon=1.3$ are constants [16]. The terms $T_{gp}^{(k)}$ and $T_{gp}^{(\varepsilon)}$ represent interphase transfer for k and ε respectively, however these are omitted in CFX 5.7.1 [17].

Generation of Turbulent Energy

$$P_{kg}=\mu_{tg}\nabla U_g\cdot\left(\nabla U_g+\nabla U_g^T\right)-\frac{2}{3}\nabla\cdot U_g\left(3\mu_{tg}\nabla\cdot U_g+\rho_g k_g\right)+P_{kbg} \tag{11}$$

Buoyancy Turbulence

$$P_{kbg}=-\frac{\mu_{tg}}{\rho_g}g\cdot\nabla\rho_g \tag{12}$$

Dispersed Phase Turbulence Model (Zero-Equation model)

$$\mu_{tp}=\frac{\rho_p}{\rho_g}\mu_{tg} \tag{13}$$

3.2.1. Boundary conditions

The gas velocity at the inlet to the duct was specified at the experimental conditions and at the solids inlet, the mass flow rate, velocity

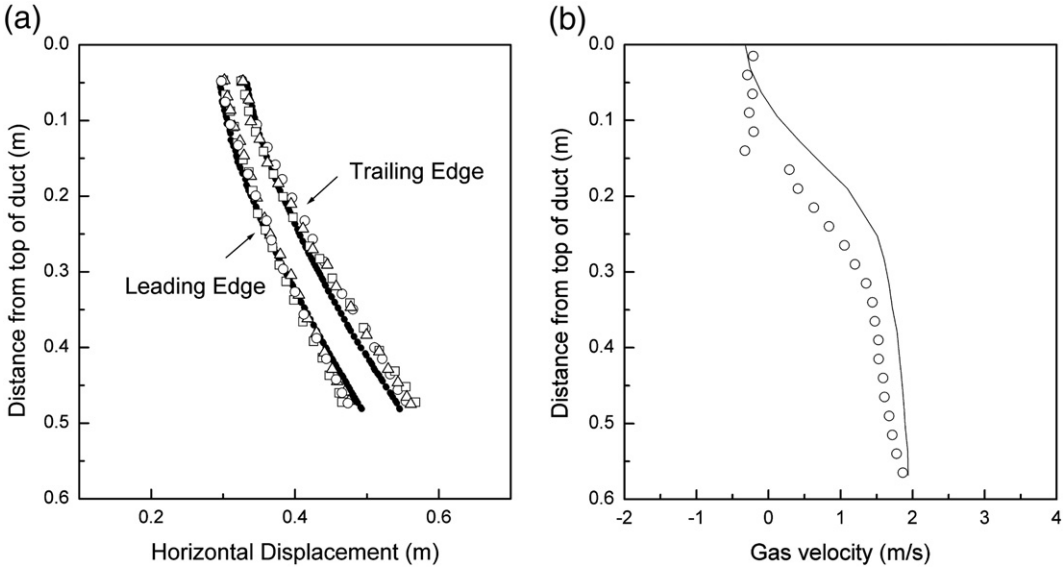

Fig. 7. (a). Particle curtain trajectories for particle curtain with inlet thickness of 2 cm, solid mass flowrate of 0.040 kg/s, and air velocity of 1.2 m/s (○ Run 1, □ Run 2, Δ Run 3, — CFD model). (b). Gas velocity profile at the trailing edge for particle curtain with inlet thickness of 2 cm, solid mass flowrate of 0.040 kg/s, and air velocity of 1.2 m/s (○ measured, — CFD model).

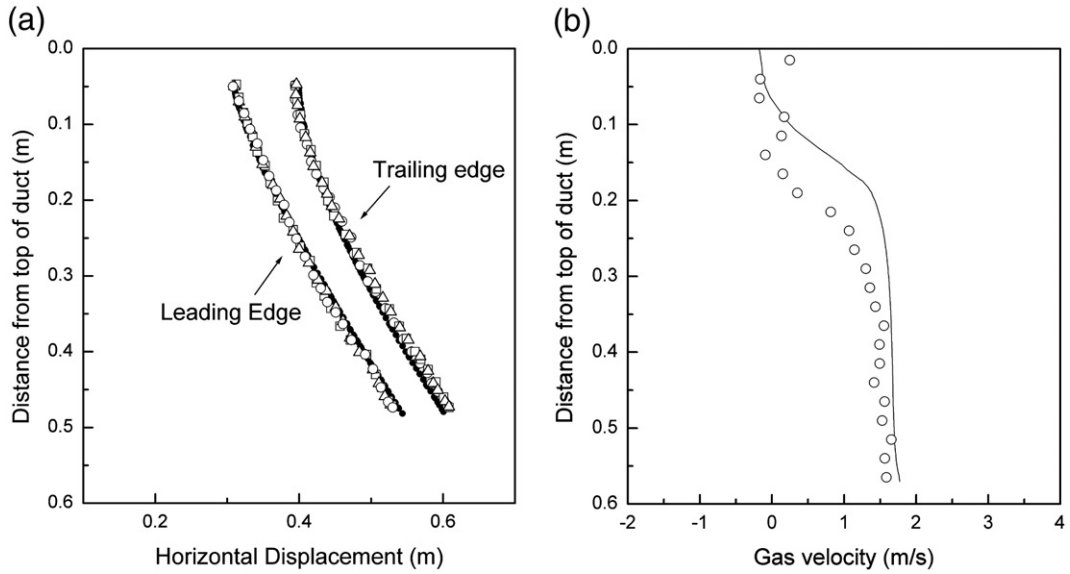

Fig. 8. (a). Particle curtain trajectories for particle curtain with inlet thickness of 10 cm, solid mass flowrate of 0.040 kg/s, and mean gas velocity of 1.2 m/s (○ Run 1, □ Run 2, Δ Run 3, — CFD model). (b). Gas velocity profile at the trailing edge for particle curtain with inlet thickness of 10 cm, solid mass flowrate of 0.040 kg/s, and mean gas velocity of 1.2 m/s (○ measured, — CFD model).

and initial voidage of the solids were specified. The inlet voidage of material was calculated based on experimental data using the following equation $r_{p0} = \frac{\dot{M}_p}{\rho_p U_0 A}$, where $\dot{M}_p$ is the mass flow rate of solids entering the system, U_{p0} is the initial velocity of the solids entering the duct, and A is the cross-sectional area of the solids inlet.

At the downstream end of the duct, the boundary was defined as an outlet boundary, such that the material can only exit the system through this boundary. In the absence of experimental data, the gas and solids inlets were given a turbulence intensity of 5% [18]. The remaining boundary conditions were governed by the no-slip condition.

3.2.2. Analysis of results

The results of the simulations were analysed using CFX 5.7.1 post-processor. The edges of the curtain were defined using a contour of constant solids volume fraction in the simulated results. Comparing the results of the simulations to the experimental data, where it was found that the lowest contour, with a solids volume fraction of 5.6×10^{-4}, corresponded well with the experimentally measured results. Measurements of other variables in the system were taken at the same location as the physical measurements in the experiments.

4. Results and discussion

Figs. 5–10 show (a) the trajectories of leading and trailing edges of the particle curtain and (b) the downstream gas velocity profiles of the particle curtain for a range of conditions. The reproducibility of the experimental measurements was found to be good, as can be seen from the small degree of scatter in all the repeated experiments.

Figs. 5(a) and 6(a) show the influence of increasing initial curtain thickness on the curtain trajectory at an air velocity of 0.9 m/s and solids mass flow rate of 0.040 kg/s. Figs. 7(a) and 8(a) allow the same comparison at an air velocity of 1.2 m/s. When the inlet particle curtain thickness is set to 2 cm, the particle curtain, viewed in

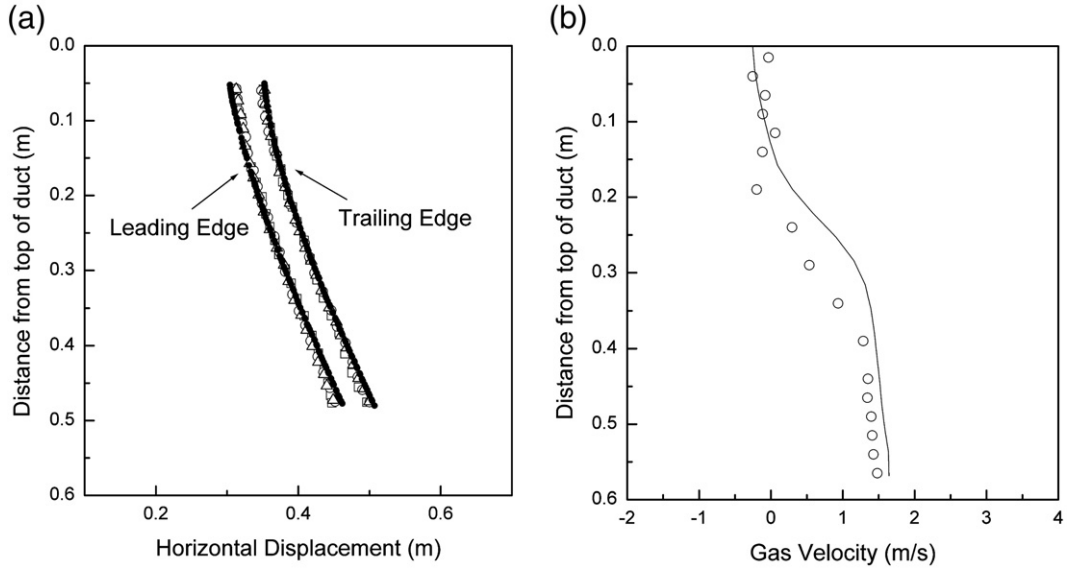

Fig. 9. (a). Particle curtain trajectories for particle curtain with solid mass flowrate of 0.031 kg/s, inlet thickness of 5 cm, and air velocity of 0.9 m/s (○ Run 1, □ Run 2, Δ Run 3, — CFD model). (b). Gas velocity profile at the trailing edge for particle curtain with solid mass flowrate of 0.031 kg/s, inlet thickness of 5 cm, and air velocity of 0.9 m/s (○ measured, — CFD model).

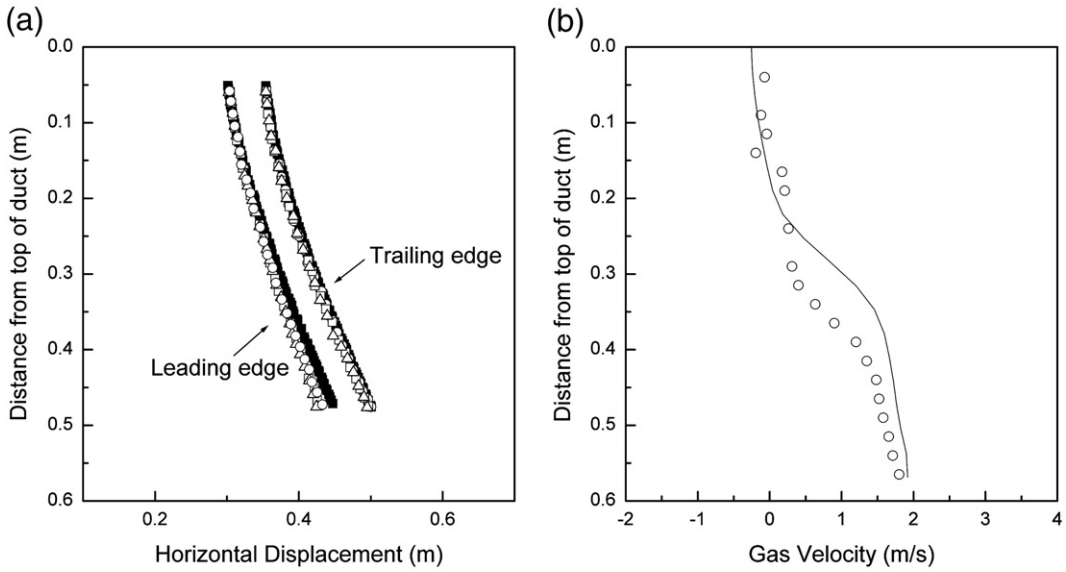

Fig. 10. (a). Particle curtain trajectories for particle curtain with solid mass flowrate of 0.047 kg/s, inlet thickness of 5 cm, and air velocity of 0.9 m/s (○ Run 1, □ Run 2, Δ Run 3, — CFD model). (b). Gas velocity profile at the trailing edge for particle curtain with solid mass flowrate of 0.047 kg/s, inlet thickness of 5 cm, and air velocity of 0.9 m/s (○ measured, — CFD model).

elevation, was found to diverge as it falls. When the inlet curtain thickness was increased to 10 cm, the particle curtain was found to converge as it falls. The converging and diverging effect had been observed by other particle curtain studies in quiescent air [19,20].

Figs. 5(b)–10(b) shown that the air velocity profile downstream of the particle curtain was far from uniform. The experimental results from these figures clearly showed that no gas is flowing at the top section downstream of the curtain. The acceleration of the particles as they fall results in an increasing void fraction with increasing distance from the solids feed point. This results in more gas passing through the lower part of the curtain than passes through the upper part.

Figs. 5(b)–10(b) also shown the comparisons of experimentally measured gas velocities with the gas velocities predicted by the CFD model at the downstream of the particle curtain. The CFD model was able to predict the trends of the experimental gas velocities. The discrepancy between the experimental result and the CFD as shown in Figs. 5(b)–10(b) was due to the uncertainty in the exact location for the gas velocity measurement.

Figs. 9(b) and 10(b) show the influence of increasing solid mass flowrate on the air velocity profile downstream of the particle curtain at an air velocity of 0.9 m/s and inlet curtain thickness of 5 cm. When the solid mass flowrate was increased from 0.031 kg/s [Fig. 9(b)] to 0.047 kg/s [Fig. 10(b)], the increase of gas flow occurs further towards the base of the duct (i.e. gas is entrained for longer).

In Figs. 5–10 experimentally measured trajectories of leading and trailing edges of particle curtain are compared with the trajectories based on the CFD model prediction. In each case, both the leading and trailing edge of the curtain are well predicted by the CFD model. The predictions of the simple single particle model for the trajectories of leading and trailing edge of particle curtain are compared with experiment in Figs. 11 and 12. Though the trends are reproduced reasonably well, the agreement is generally poor. The likely reason for

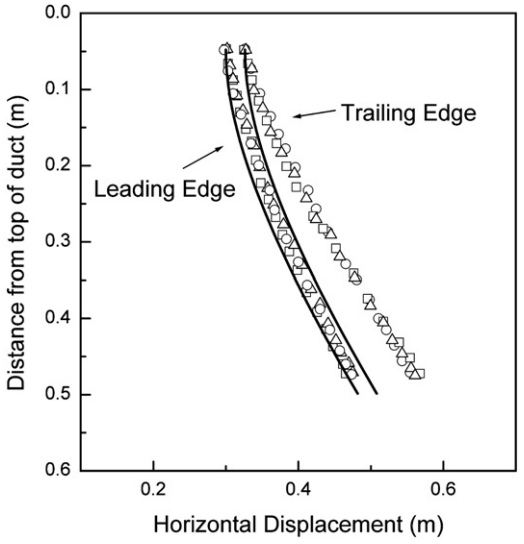

Fig. 11. Particle curtain trajectories for gas velocity of 1.2 m/s, curtain thickness of 2 cm, and solid mass flowrate of 0.040 kg/s (○ Run 1, □ Run 2, Δ Run 3, — single particle model).

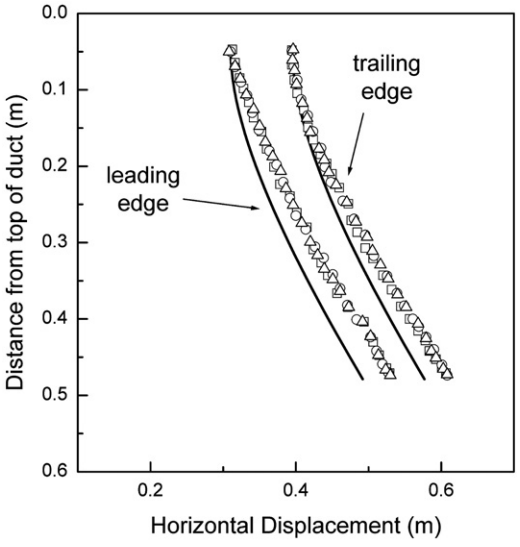

Fig. 12. Particle curtain trajectories for gas velocity of 1.2 m/s, curtain thickness of 10 cm, and solid mass flowrate of 0.040 kg/s (○ Run 1, □ Run 2, Δ Run 3, — single particle model).

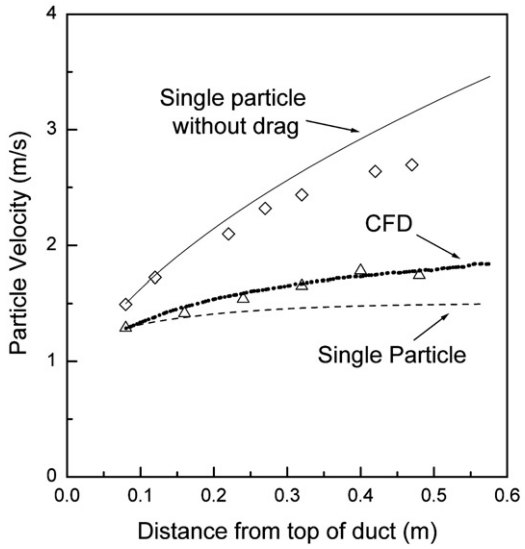

Fig. 13. Particle velocity profile with 10 cm curtain thickness and solid mass flowrate of 0.040 kg/s (◊ in quiescent air, Δ in horizontal gas flow 0.9 m/s).

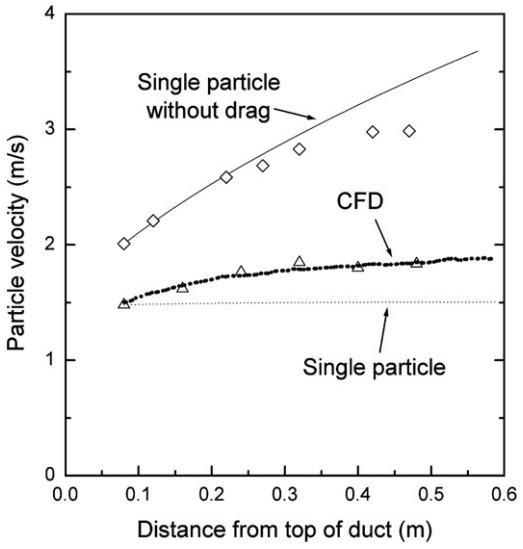

Fig. 14. Particle velocity profile with 2 cm curtain thickness and solid mass flowrate of 0.040 kg/s (◊ in quiescent air, Δ in horizontal gas flow 0.9 m/s).

this poor agreement is that the simple model assumes uniform air flow through the entire curtain, whereas measurements [Figs. 5b–10b], reinforced by the CFD analysis, show that this assumption is not true.

Fig. 13 shows the measured vertical component of particle velocity at the centerline of the particle curtain as a function of falling distance for quiescent air and for an air velocity of 0.9 m/s, with an initial curtain thickness of 10 cm. The measured values with horizontal air flow are compared with the CFD model prediction and the simple single particle drag model prediction. The measured velocity in quiescent air is compared with the calculated particle velocity without drag (free-fall without drag). Fig. 14 shows the same for an initial curtain thickness of 2 cm. In both cases, the single particle drag model underestimates the measured velocity with horizontal air flow, whereas the CFD model gives good agreement.

The CFD model gives a good prediction of the centerline particle velocity within the curtain falling in a horizontal air flow. The single particle model overestimates the drag on the particles within the curtain and so underestimates the centerline particle velocity within the curtain falling in a horizontal air flow. For the motion in quiescent air, in the upper part of the curtain the centerline particle velocity approaches that of a single particle (any other object) falling under gravity without drag. In the lower part of the curtain the centerline velocity starts to deviate from the "no drag" velocity. This is probably due to the increased void fraction (as a result of particle acceleration) causing increased drag. The smaller initial curtain thickness [Fig. 14] gives a closer approach to the "no drag" velocity — due to lower initial void fraction and resultant lower initial drag. These findings compare well with those of Ogata et al. [5].

5. Conclusion

An experimental study of the fluid dynamic behaviour of a particle curtain falling through a horizontal air flow is presented. The particle curtain spanned the entire width of the vessel, with no free space between the curtain and the duct walls, thus forcing the gas to flow through the curtain. The trajectory of the particle curtain was tracked using high-speed video and compared with CFD simulations and a simple single particle model. Good agreement was found between the experiments and the CFD model predictions, however the predictions of the simple single particle model were less satisfactory. This is thought to be primarily due to the non-uniform gas flow found in practice, due to the entrainment of gas within the falling curtain of solids, as opposed to the uniform gas flow assumed by the single particle model.

Nomenclature

C_D	drag coefficient
d	diameter, m
g	gravitational acceleration, m/s^2
k	turbulence kinetic energy per unit mass, m^2/s^2
P	pressure, Pa
P_k	turbulence production due to viscous and buoyant forces, kg/m s^3
P_{kb}	turbulence production due to buoyant forces, kg/m s^3
r	volume fraction, m^3/m^3
r_{pm}	maximum solids volume fraction, m^3/m^3
Re	Reynolds number $\left(\frac{\rho_g(\dot{y}_p-\dot{y}_g)d_p}{\mu_g}\right)$
T	Temperature, K
$T_{gp}^{(k)}$	interphase turbulent kinetic energy transfer term
$T_{gp}^{(\varepsilon)}$	interphase turbulence dissipation transfer term
$\dot{x}$	particle velocity in x-direction, m/s
x	particle acceleration in x-direction, m/s^2
$\dot{y}$	particle velocity in y-direction, m/s
$\ddot{y}$	particle acceleration in y-direction, m/s^2
ε	turbulence dissipation rate, m^2/s^3
μ	dynamic viscosity, kg/m s
μ_t	turbulent dynamic viscosity, kg/m s
ρ	density, kg/m^3
ρ_{ref}	reference gas density calculated at the centre of the duct outlet, kg/m^3

Subscripts

p	particle
g	gas

References

[1] S. Ouyang, Q.M. Mao, M. Rhodes, O.E. Potter, Short contact time gas–solid systems, Reviews in Chemical Engineering 19 (2) (2003).
[2] A.R. Shirley Jr., L.M. Nunnelly, F.T. Carney Jr., Melt granulation of urea by the falling-curtain process, Industrial & Engineering Chemistry Product Research and Development 21 (1982) 617–620.
[3] J. Hruby, R. Steeper, G. Evans, C. Crowe, An experimental and numerical study of flow and convective heat transfer in a freely falling curtain of particles, ASME Journal of Fluids Engineering 110 (1988) 172–181.

[4] T. Uchiyama, Numerical analysis of particulate jet generated by free falling particles, Powder Technology 145 (2004) 123–130.
[5] K. Ogata, K. Funatsu, Y. Tomita, Experimental investigation of a freely falling powder jet and the air entrainment, Powder Technology 115 (2001) 90–95.
[6] J.J. Kelly, P. O'Donnell, Dynamics of granular material in rotary drier and coolers, Institution of Chemical Engineers Symposium Series 29 (1968) 34–44.
[7] F.A. Kamke, J.B. Wilson, Computer simulation of a rotary dryer part I: retention time, AIChE Journal 32 (1986) 34–44.
[8] J.J. Kelly, P. O'Donnell, Residence time model for rotary drums, Trans IChemE 55 (1977) 243–252.
[9] R.G. Sherritt, R. Caple, L.A. Behie, A.K. Mehrotra, The movement of solids through flighted rotating drums, part II: solids–gas interaction and model validation, Canadian Journal of Chemical Engineering 72 (1994) 240–248.
[10] W. Du, X. Bao, J. Xu, W. Wei, Computational Fluid Dynamics (CFD) modelling of spouted bed: assessment of drag coefficient correlations, Chemical Engineering Science 61 (2006) 1401–1420.
[11] H. Nakamura, S. Watano, Numerical modelling of particle fluidization behaviour in a rotating fluidized bed, Powder Technology 171 (2007) 106–117.
[12] M. Hidayat, R. Rasmuson, Some aspects on gas–solid flow in a U-bend: numerical investigation, Powder Technology 153 (2005) 1–12.
[13] S. Cooper, C.J. Coronella, CFD simulations of particle mixing in a binary fluidized bed, Powder Technology 151 (2005) 27–36.
[14] L. Schiller, A. Naumann, Über die grundlegenden berechungen bei der schwerkraftaufbereitung, Vereines Deutscher Ingenieure 77 (1933) 318–320.
[15] T. Norton, D.W. Sun, Computational Fluid Dynamics (CFD) — an effective and efficient design and analysis tool for the food industry: a review, Trends in Food Science and Technology 17 (2006) 600–620.
[16] B.E. Launder, D.B. Spaulding, Lectures in Mathematical Models of Turbulence, Academic Press, 1972.
[17] CFX Solver Theory Guide, Ansys Europe, Ltd., 2006.
[18] CFX Solver Modelling Guide, Ansys Europe, Ltd., 2006.
[19] P. Wypych, D. Cook, P. Cooper, Controlling dust emissions and explosion hazards in powder handling plants, Chemical Engineering and Processing v44 (2005) 323–326.
[20] R.C. Darton, The structure and dispersion of jets of solid particles falling from a hopper, Powder Technology v13 (1976) 241–250.
[21] D.A. Wegerer, Short Contact FCC Process with Catalyst Blending, US Patent 5462652, 1995.